

Automated derivation of stellar atmospheric parameters and chemical abundances: the MATISSE algorithm.

A. Recio-Blanco¹, A. Bijaoui¹ and P. de Laverny¹ \star

¹*Dpt. Cassiopée, UMR 6202, Observatoire de la Côte d'Azur, B.P.4229, F-06304 Nice Cedex 4, France*

Accepted Year Month day. Received 2005 Month day; in original form 2005 Month day

ABSTRACT

We present an automated procedure for the derivation of atmospheric parameters (T_{eff} , $\log g$, $[M/H]$) and individual chemical abundances from stellar spectra. The MATrix Inversion for Spectral SythEsis (MATISSE) algorithm determines a basis, $B_{\theta}(\lambda)$, allowing to derive a particular stellar parameter θ by projection of an observed spectrum. The $B_{\theta}(\lambda)$ function is determined from an optimal linear combination of theoretical spectra and it relates, in a quantitative way, the variations in the spectrum flux with variations in θ . An application of this method to the GAIA/RVS spectral range is described, together with its performances for different types of stars of various metallicities. Blind tests with synthetic spectra of randomly selected parameters and observed input spectra are also presented. The method gives rapid, accurate and stable results and it can be efficiently applied to the study of stellar populations through the analysis of large spectral data sets, including moderate to low signal to noise spectra.

Key words: stars: abundances - stars: fundamental parameters - methods: data analysis - techniques: spectroscopy - Galaxy: stellar content

1 INTRODUCTION

The physical parametrization of stars is a crucial step in our comprehension of stellar and galactic astrophysics. By way of illustration, it could be cited the impact of the Hertzsprung-Russel (HR) diagram on our understanding of stellar evolution, or the identification and characterization of the different components and stellar populations of the Milky Way and its satellites. The classification of stars, from rich collections of stellar properties and vast catalogues of objects, is now opening new horizons in, for instance, the disentangling of the detailed sequence of events which led to the Milky Way galaxy. In this sense, the chemical parametrization of stars is mandatory for a fruitful classification attempt, reinforcing the traditional approach. The chemical abundance ratios of some species to others (e.g. the $[\alpha/Fe]$ ratio) provide an indication of the star formation history time scale and details of the chemical enrichment for one specific population.

In the recent years, the use of spectrographs with multi-object capabilities (FLAMES, 2dF...) and the implementation of extensive surveys (Sloan, RAVE,...) has enormously increased the quantity of available data and, as a result, the efforts needed for their analysis. In the near future, the Eu-

ropean Space Agency Gaia mission will collect several millions of stellar spectra, allowing a very complete mapping of the Milky Way. Moreover, thanks to the spectral resolution ($R=11\,500$) of the Gaia Radial Velocity Spectrograph (RVS), it will be possible to derive individual chemical element abundances, leading to a huge and precious database. In this context, automated techniques of spectral analysis and classification are needed, in order to perform a rapid and homogeneous processing of the data and to allow an efficient scientific return.

The intrinsic physical properties of stars, can be indirectly derived from stellar spectra. Effective temperature (T_{eff}), surface gravity ($\log g$), and chemical composition are the main parameters governing the stellar atmosphere and non-linear combinations of them characterize the features on a stellar spectrum. The knowledge of these quantities, together with stellar structure and evolution models, can help to determine a star's history and future evolution.

Traditionally and for historical reasons, the more empirical variables of luminosity and colour index have been used to indirectly describe spectroscopic parameters. The MK system (Morgan, Keenan & Kellman, 1943) avoids the complexities of spectral lines formation by the use of standard spectra. Spectral class and luminosity type are assigned from medium-low resolution spectra in, essentially, a two-parameters classification effort, representative of T_{eff} and $\log g$. Nevertheless, this approach suffers from a series of

\star E-mail: arecio@obs-nice.fr, bijaoui@obs-nice.fr, laverny@obs-nice.fr

disadvantages, mainly arising from the lack of a metallicity quantification. The almost neglect of the chemical dimension is the cause of an important loss of scientific information. Moreover, since the match between the object spectrum and the MK standards is visually performed, the classification suffers from subjective decisions.

On the other hand, a classification directly based on the physical parameters, although model dependent, takes more naturally into account the scientific quantities of interest and offers a continuous parametrization instead of a discrete spectral/luminosity type assignment.

We describe here the MATrix Inversion for Spectral SythEsis (MATISSE) algorithm. It represents a new effort in automatic spectral analysis (for discussion of already developed methods see Bailer-Jones, 2001). The parametrization problem, applicable to millions of stellar spectra, is approached in a way that tries to tackle some disadvantages of already existing automated classification techniques, as excessive computing times. This method uses the inversion of the covariance matrix of a grid of synthetic spectra to determine a basis allowing to derive a particular stellar parameter by projection of an object spectrum. An initial attempt was reported by Thévenin, Bijaoui & Katz (2002).

The motivation and the mathematical description of the method are developed in Section 2. Section 3 presents all the steps in the application of MATISSE and the results on the measurement of stellar atmospheric parameters (T_{eff} , $\log g$, global metallicity [M/H]) and $[\alpha/\text{Fe}]$ abundance for stars in different parts of the Hertzsprung-Russel diagram. The procedure performances are illustrated for input data in the Gaia/RVS wavelength domain, including real spectra. Final discussions and conclusions are presented in Section 4.

2 MATHEMATICAL BASE OF THE MATISSE ALGORITHM

Let us consider an observed spectrum $O(\lambda)$, corrupted by a Gaussian noise, independent of λ , of standard deviation σ . A grid of theoretical spectra $S(\lambda, \theta)$, where θ corresponds to the stellar parameters, is implemented for its analysis. In this framework, the parameters estimation problem consists into finding the minimum distance $d(\theta)$ between $O(\lambda)$ and the spectra $S(\lambda, \theta)$. It is a typical least mean square estimation problem. Its classical solution is obtained by solving the normal equations resulting from the $d(\theta)$ derivation as a function of each parameter. Nevertheless, many problems arise from this approach:

- Stellar spectra do not depend linearly on the physical parameters, so that an iterative procedure must be done, using a local linearization.
- The synthetic spectra are previously computed on a set of discrete parameters. The iterative procedure needs to compute many models with enough resolution for the targeted precision. Generally, this operation can not be done. The estimation can be only obtained from a set of given models.
- The distance is not necessarily a convex function of the parameters. So the gradient descent can lead to a local minimum, far from the correct one.

As a consequence, instead of solving the normal equations after linearization, it is better, for a given set of models, to find directly the minimum by i) computing all the distances to the models and ii) interpolating between the distances corresponding to the neighbour parameter values (limiting the computations to a restricted cell of models). This approach needs the computation of a theoretical grid with the enough resolution to get a convex function for the distance, in the volume restricted to each cell. Within a cell, the spectral distribution should be *quasi* linear as a function of the parameters. This insurance can not be obtained by theoretical derivations but by experimentation. In this situation, the determination of the set of parameters, corresponding to the minimum distance, leads to a solution with the accuracy of the grid resolution. Therefore, the problem consists into increasing the accuracy without computing new models.

Already existent automatic classification methods, mainly minimum distances techniques, genetic algorithms and neural networks, try to tackle the above described problem in different ways (see also examples in Sect. 4), none of them without disadvantages.

As mentioned before, pure minimum distances methods are limited by the theoretical spectra grid resolution. Moreover, border effects with respect to the selected grid can be considerable. The time for the data processing is also heavy, when dealing with a grid of several thousand elements. Genetic algorithms can also suffer from excessive computing times, critical dependences on the algorithm parametrization and difficulties in evaluating the suitability of the final convergence. Finally, in neural networks methods, the individual relations between the input variables and the output variables have not an analytical basis. As a consequence, the impact of the underlying physical laws and parameters is more difficult to estimate. In addition, they need a hierarchical structure that is unknown *a priori*.

In this context, the method presented here opens an unexplored pathway. Two approaches were initially examined, in order to solve the interpolation problem described above:

- The objective analysis (Recio-Blanco et al., 2005), which determines a parameter through a weighted combination of the corresponding cell values. The weights are derived from the distances between the observed spectrum and the models. Exponential weights gave the best results. Nevertheless, the results were not very satisfying. In particular, a bias appeared for values near the limits of the grid, as for classical minimum distances techniques.
- An algorithm based on the projection of the observed spectrum on specific basic vectors. These vectors are a combination of the neighbour models. This algorithm, MATISSE, carried out to the best results and is described below.

The idea of the MATISSE algorithm came from the classical Principal Component Analysis (PCA). From the PCA we get a set of decorrelated components as combinations of the measurements (in our problem the spectral intensities). The weights of the combinations are the eigenvectors of the variance-covariance matrix. One could imagine that the principal components would correspond also to physical parameters. The experiments showed that it was not true. So, the question was to derive the weights which gives coefficients as close as possible to the physical parameters. The

criterion we adopted was the statistical correlation between the input and the output parameter values.

In other words, the implemented algorithm determines a vector, $B_\theta(\lambda)$, allowing to derive a particular stellar parameter θ by projection of an input spectrum on it. This θ parameter can be the effective temperature, the gravity, the global metallicity, the $[\alpha/\text{Fe}]$ content, individual chemical abundances, $v \sin i$ value, etc... The $B_\theta(\lambda)$ function is derived from an optimal linear combination of theoretical spectra and it relates, in a quantitative way, the variations in the spectrum flux with the θ variations.

First of all, the data on a particular θ variable and the spectra of the grid are subtracted of their mean value. The $B_\theta(\lambda)$ basis is then constructed from a linear combination of spectra, with α_i being the weight associated to the spectrum $S_i(\lambda)$:

$$B_\theta(\lambda) = \sum_i \alpha_i S_i(\lambda) \quad (1)$$

The parameter θ_i is estimated by the projection of a spectrum into the corresponding basis vector:

$$\hat{\theta}_i = \sum_\lambda B_\theta(\lambda) S_i(\lambda) \quad (2)$$

with $\hat{\theta}_i$ being the recovered value.

Combining Eq. 1 and Eq. 2 we obtain :

$$\hat{\theta}_i = \sum_j c_{ij} \alpha_j \quad (3)$$

where c_{ij} is the correlation value between the spectra S_i and S_j . Taking into account that the spectra have been subtracted of their mean value, c_{ij} can be interpreted as the covariance between the S_i and S_j , if the spectral values are considered as random variables.

The α_i are obtained from the maximum correlation between θ_i and $\hat{\theta}_i$. Therefore, the following relation:

$$R = \frac{(\sum_i \hat{\theta}_i \theta_i)^2}{\sum_i \hat{\theta}_i^2} \quad (4)$$

has to be maximized. Using Eq. 3, the above expression can be written in the form:

$$R = \frac{(\sum_j \alpha_j (\sum_i c_{ij} \theta_i))^2}{\sum_{j,k} (\alpha_j \alpha_k (\sum_i c_{ij} c_{ik}))} \quad (5)$$

Hence, maximizing R we obtain:

$$\sum_k (\sum_i c_{ij} c_{ik}) \alpha_k = a (\sum_i c_{ij} \theta_i) \quad (6)$$

with a being a scalar quantity that we can impose to be equal to 1. Therefore, for an invertible covariance matrix, we would have:

$$\sum_k c_{ik} \alpha_k = \theta_i \quad (7)$$

In our case, the covariance matrix is empirically found to be non invertible. As a consequence, Eq. (6) has to be solved through a least squares linear regression between θ and $\hat{\theta}$. The optimal α_i values can be calculated, for instance, from an iterative Van Cittert's algorithm (Van Cittert, 1931).

In other words, we determine a linear relation between the values of a parameter θ_i for a given set of spectra, $S_i(\lambda)$, and the product $S_i(\lambda) B_\theta(\lambda)$.

Then, to determine the parameters of an object spectrum, not belonging to the learning set, it is only necessary to multiply it by the corresponding $B_\theta(\lambda)$ and to transform the result using the derived linear regression between $\hat{\theta}$ and θ . This procedure is therefore extremely rapid and ideal for the analysis of huge quantities of data.

In order to avoid the effects of important non-linear variations in the spectra, it is advisable to restrict the working domain to a subregion of the spectra grid. To this purpose, a two level procedure can be followed, by deriving initial $B_\theta^0(\lambda)$ functions to make a preliminary guess in the parameters and then to refine the result using local $B_\theta^l(\lambda)$ functions (see Section 3.2). This initial guess can also be done through the evaluation of available photometry for the targets.

3 APPLICATION OF MATISSE TO SPECTRA IN THE GAIA RVS DOMAIN

In order to illustrate the performances of the algorithm, this Section describes its application to the measurement of stellar atmospheric parameters (T_{eff} , $\log g$, $[\text{M}/\text{H}]$) and $[\alpha/\text{Fe}]$ abundance for stars in different parts of the Hertzsprung-Russel diagram. The Gaia/RVS spectral domain has been selected as the framework for this example, due to its large potential in the analysis of stellar spectra for Galactic studies (Munari, 2003 and the RAVE consortia studies). It ranges from λ 8470-8740 Å, containing the infrared triplet of ionized calcium. Thanks to the RVS spectral resolution, $R=11\,500$, several atomic and molecular lines, depending on stellar spectral type and signal to noise ratio, can be identified. The most relevant features in the RVS wavelength range are the ionized calcium triplet lines, together with the hydrogen Paschen lines. Many lines of iron and iron peak elements can also be found. Moreover, besides of calcium, other α -elements like silicium, sulfur, magnesium and titanium have features in the RVS range. One s-process element, the zirconium, has one measurable line in the appropriate conditions of signal to noise and atmospheric parameters. Finally, molecular lines, like the TiO and CN lines, are detectable for the coolest stars.

All the steps in the application of MATISSE are described below, including the used synthetic spectra grid. The procedure performances are detailed through the results for trial spectra and blind tests with unknown input flux calibrated (Sect. 3.3) and normalized (Sect. 3.4) spectra.

3.1 The grid of synthetic stellar spectra

The computed grid of theoretical stellar spectra covering the Gaia/RVS domain (see Recio-Blanco, de Laverny & Plez, 2005, for a more detailed description) is based on a new generation of MARCS model atmospheres and mostly devoted to FGK dwarf and giant stars. It was computed with the turbospectrum code (Alvarez & Plez 1998, and further improvements by Plez) in plane-parallel and spherical geometry (depending on the gravity).

The adopted line list consists in all the atomic lines

found in the VALD database (Kupka et al., 1999) and molecular lines. The molecular line list includes ZrO, TiO, VO, CN, C₂, CH, SiH, CaH and MgH lines with their corresponding isotopic variations. Collisional broadening by atomic hydrogen of several atomic lines are computed as in Barklem et al. (2000). Other lines are broadened with the classical theory (see Recio-Blanco, de Laverny & Plez, 2005, for further details about these linelists). We note that the treatment of the line broadening is an important issue when comparing synthetic to observed spectra and that could introduce some biases in the derived atmospheric parameters. However, this article is focussed on a new algorithm for the derivation of such parameters and its internal validity is actually independent of that issue.

Regarding the model atmospheres, we used a new grid of MARCS (version of November 2004) one-dimensional, plane-parallel and spherical LTE model atmospheres (Gustafsson et al., 2003; Gustafsson et al., 2006). Turbulence pressure was included and convection was simulated according to the local mixing-length recipe. The grid consists in 1 858 stellar models with effective temperatures between 4 000 K and 8 000 K (step 250 K), logarithmic surface gravities between -1.0 to 5.0 (step 0.5), and overall metallicities between -5.0 and 1.0 (with a variable step from 1.0 to 0.25 dex) and different α -element enhancements (see below). The adopted solar abundances for C, N and O in the atmospheric models are from the recent revision by Asplund et al. (2005). Solar abundances of other chemical species are from Grevesse & Sauval (1998).

From this grid of model atmospheres, synthetic spectra have been computed in the range $\lambda = 8475\text{\AA}$ to $\lambda = 8745\text{\AA}$ with a step of 0.02\AA and then convolved and re-sampled to match the RVS spectral resolution ($R \sim 11\,500$). The number of pixels per resolution element is 3, and for historical reasons, slightly different from the one presently defined for Gaia (2 pixels for resolution element).

The synthetic spectra have been computed with the same geometry and abundances as in the model atmosphere. Plane-parallel models have been used for $\log g$ from +3.0 to +5.0. They have a microturbulent-velocity parameter of 1.0 km/s. Models with spherical geometry have been considered for giant stars with $\log g < +3.0$. These models have been computed for masses of $1.0 M_{\odot}$ and with a microturbulence parameter of 2.0 km/s. For metal-poor models, the following α -enhancements were considered: $[\alpha/\text{Fe}] = +0.1$ for $[\text{Fe}/\text{H}] = -0.25$, $[\alpha/\text{Fe}] = +0.2$ for $[\text{Fe}/\text{H}] = -0.5$, $[\alpha/\text{Fe}] = +0.3$ for $[\text{Fe}/\text{H}] = -0.75$ and $[\alpha/\text{Fe}] = +0.4$ for $[\text{Fe}/\text{H}] \leq -1.00$. Chemical species treated as α -elements are Ne, Mg, Si, S, Ar, Ca and Ti. Oxygen also follows the same enhancements.

For each model atmosphere, we furthermore considered α -elements abundance variations of +0.4, +0.2, +0.0, -0.2, -0.4 dex, with respect to the original abundances in the model. Five synthetic spectra have thus been computed per model atmosphere leading to a final library of 9 290 spectra.

On the other hand, we point out that this grid of spectra is not optimized for all types of stars. In particular, we did not check the validity of all the considered line data and the classical assumptions (LTE, hydrostatic), used when deriving the atmospheric structure, can be questioned. However, a comparison of some synthetic spectra with observed ones shows a rather good match in the RVS domain. Finally, for the purpose of this work, the use of high quality

synthetic spectra (still not available for almost any region in the Hertzsprung-Russel diagram) is not imperative, since we focus on the algorithm itself.

3.2 Derivation of the $B_{\theta}(\lambda)$ functions

One of the advantages of the MATISSE algorithm with respect to other automatic spectral parameters derivation procedures is the fact that the calculated $B_{\theta}(\lambda)$ functions allow the control of the spectral features involved in the analysis. Basically, $B_{\theta}(\lambda)$ deviates more from zero at the wavelengths mostly affected by a change in θ , that is, at the spectral regions containing the highest quantity of information on a given parameter for the stellar types considered in the spectra grid. In this way, we are informed on which lines are been used for each parameter under consideration, in a more physical approach close to the traditional spectral synthesis. Similarly, if we prefer to avoid the use of a certain line due, for instance, to problems of unreliable atomic data, we can exclude the corresponding wavelength region from the algorithm that calculates the $B_{\theta}(\lambda)$ functions.

As a way of illustration, Figure 1 shows the derived $B_{\theta}(\lambda)$ functions for a solar type star, corresponding to the determination of effective temperature, $B_{T_{\text{eff}}}(\lambda)$, surface gravity, $B_g(\lambda)$, global metallicity, $B_M(\lambda)$ and α -element abundance with respect to iron, $B_{\alpha}(\lambda)$. These functions have been calculated for a subgrid of synthetic spectra around the point with $T_{\text{eff}} = 5750$ K, $\log g = 4.5$ dex, $[\text{M}/\text{H}] = 0.0$ dex, $[\alpha/\text{Fe}] = 0.0$ dex. The parameter dimensions of the grid subregion are 1000 K (for $B_{T_{\text{eff}}}(\lambda)$) or 500 K (for the other three functions), 1.0 dex, 1.0 dex and 0.4 dex respectively. The most important lines in a solar type spectrum are also marked in Fig. 1.

First of all, it should be noted that the most relevant features of each $B_{\theta}(\lambda)$ correspond to typical lines of the stars under analysis: Paschen lines, CaII triplet, Fe, Si, Mg lines,... In addition, $B_{T_{\text{eff}}}(\lambda)$ has a slope, positive at lower wavelengths, that reflects the temperature dependence of the continuum flux. Several metallic lines are also good temperature indicators: FeI lines (e.g. 8484.99 \AA , 8514.08 \AA , 8582.27 \AA , 8611.81 \AA) and TiI (8518.40 \AA) with increasing intensity at higher T_{eff} ; MgI (8736.04 \AA) and SiI (8694.64 \AA) with an inverse behaviour. Of the ionized calcium triplet lines, the two reddest ones (8542.14 \AA and 8662.17 \AA), including their wings, are those containing more temperature information for this kind of stars. Finally, the Paschen lines also contribute to the temperature evaluation of a solar type spectrum.

The most important features in the $B_g(\lambda)$ function, correspond to the Paschen lines (specially Pa 14 at 8598.40 \AA), the CaII lines, the neutral magnesium lines and some iron lines like FeI 8688.64 \AA . Finally, the iron lines, together with α -element lines (the CaII triplet, magnesium and silicium) dominate the information on the stellar global metallicity and the α -element abundance.

The MATISSE algorithm performs, therefore, a sort of automated spectral synthesis, by using the more adapted lines for the derivation of each stellar parameter or chemical data.

On the other hand, it is worth noticing that, in order to better separate the influence of each parameter on the spectral lines, a $B_{\theta}(\lambda)$ function has to be built from a set of

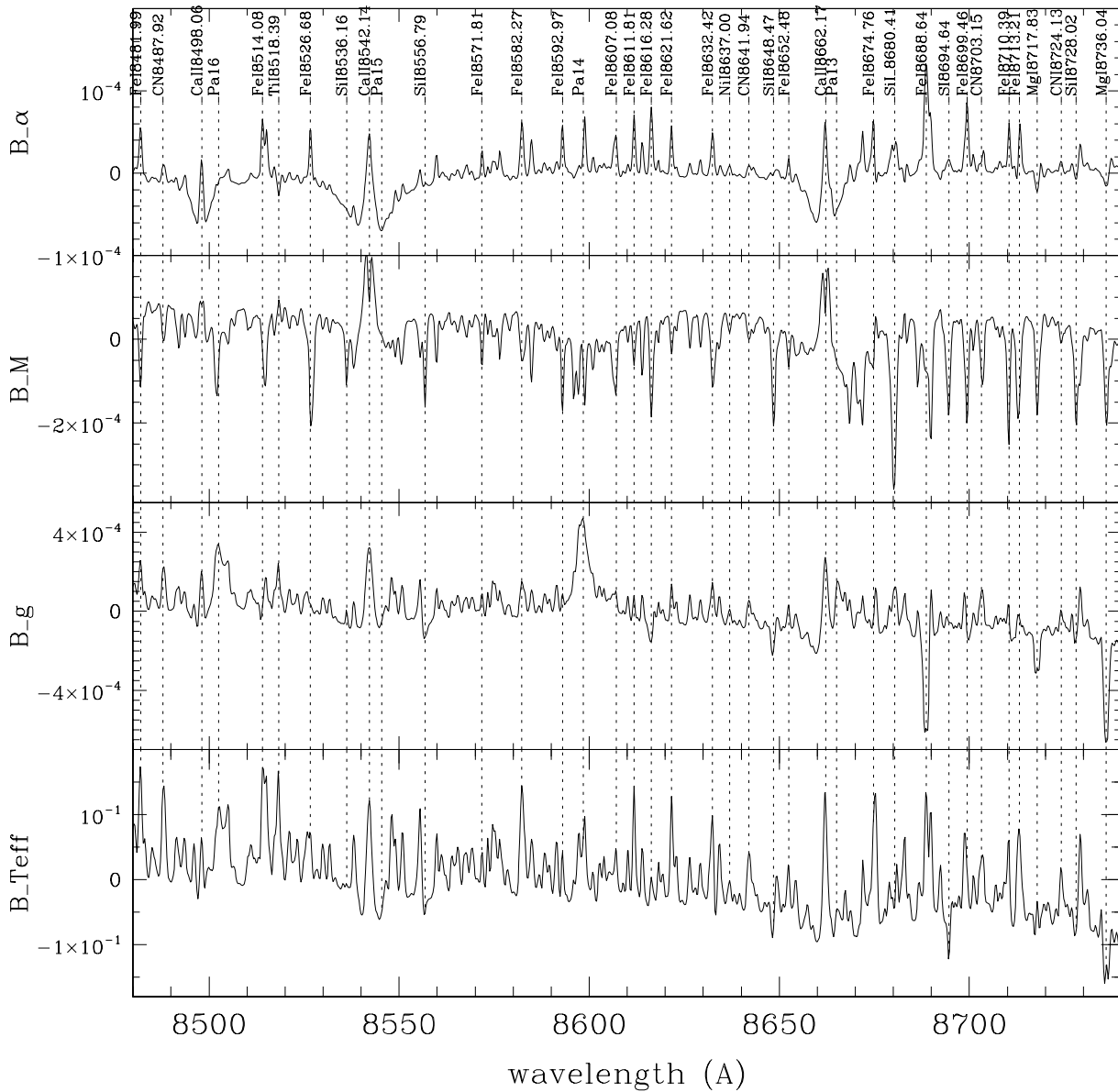


Figure 1. B functions for the effective temperature, the gravity, the global metallicity and the $[\alpha/\text{Fe}]$ content of a solar type star (the units are related to the considered parameter ones, per flux unit). The spectral lines identification in the upper panel allows to see how a particular $B_\theta(\lambda)$ function deviates more from zero at the wavelengths containing the highest quantity of information on the corresponding parameter θ .

synthetic spectra sharing at least $(D - 1)$ parameters, where D is the dimension of the grid. In other words, once the centre of the grid (or subgrid) we want to analyse is selected, only those spectra having $(D - 1)$ parameters equal to the central point have to be used. In practice, this allows to deal with spectra at varying T_{eff} but constant $\log g$, $[\text{M}/\text{H}]$ and $[\alpha/\text{Fe}]$, varying $\log g$ but constant T_{eff} , $[\text{M}/\text{H}]$ and $[\alpha/\text{Fe}]$, etc... As a consequence, it is possible to better distinguish between a change in the spectrum caused by a change in, for instance, T_{eff} , from the effect due to the variation of a different parameter.

3.3 Application to flux calibrated spectra.

To illustrate the performances of MATISSE as applied to the Gaia/RVS spectral domain and resolution, the results for trial spectra from different regions of the Hertzsprung-Russel diagram are presented in the following. In this Section, the performances on flux calibrated spectra are described. Actually, the flux calibration of the Gaia/RVS spectra will be allowed by one medium band photometric filter covering the RVS spectral range and by accurate absolute distance measurements (from parallaxes) for all the stars observed by the RVS.

In order to evaluate the performances of the method and to ensure the absence of biases and the validity of a linear treatment as the MATISSE one, the algorithm has been applied to synthetic spectra of different stellar types. This allows to confirm the stability of the method at different spectral classes, luminosity types and metallicity contents, but also to illustrate the dependencies of the obtained performances on the stellar atmospheric properties. In particular, possible tracers of the Galactic Thin disc, Thick disc and Halo stellar populations have been selected to this purpose: metal rich cool dwarfs ($T_{\text{eff}} = 5000\text{-}6000$ K, $\log g > 3.5$ dex, $[M/H] > -0.5$ dex) intermediate metallicity cool giants ($T_{\text{eff}} < 5000$ K, $\log g = 1.0\text{-}3.5$ dex, $0.0 \text{ dex} > [M/H] > -1.0$ dex) and very metal poor hot subgiants ($T_{\text{eff}} > 6000$ K, $\log g = 2.0\text{-}4.0$ dex, $-1.0 > [M/H] > -2.5$ dex). The various $[\alpha/\text{Fe}]$ contents included in the grid have been considered.

A total of 100 different cases, with randomly selected parameters, in the above ranges, have been analysed to check if the performance is the same regardless how many parameters are initialized from a position off the subgrid centre. In addition, to quantify the dependence of the results on the quality of the input spectra, a programme to introduce Gaussian white noise, at desirable values of signal to noise ratio (S/N), was implemented. For each of the 100 *object* synthetic spectra, five signal to noise values have been considered and 1000 noised spectra were computed for each S/N value. The MATISSE algorithm is then applied to a total of 500 000 spectra, in order to derive their atmospheric parameters and $[\alpha/\text{Fe}]$ abundance.

At this stage, the use of input synthetic spectra instead of a library of real data guarantees the absence of additional errors that could blur the true performances of the method (see for example Bailer-Jones, 2000 and Willemsen et al. 2003 for other works on automated spectral analysis using synthetic spectra). Actually, imperfections in the physical assumptions (LTE, hydrostatic, see for instance Asplund 2005), uncertainties in the line data used for the theoretical spectra computation, uncertainties in the parameters of the real stars, etc... could produce biases on the results and complicate the evaluation of the MATISSE procedure. In addition, the use of synthetic spectra allows the availability of a larger number of data over a large parameter space.

First of all, a preliminary evaluation of the spectrum parameters can be done using MATISSE initial $B_{\theta}^{\circ}(\lambda)$ functions. This permits to restrict the working domain to a sub-region of the spectra grid and to minimize the effects of important non linear variations in the spectra, through the considered parameter range. The preliminary values of the parameters can then be refined or corrected by using *local* $B_{\theta}^l(\lambda)$ functions.

The $B_{\theta}^{\circ}(\lambda)$ functions are derived from theoretical spectra whose parameters span the whole range of the grid or an important fraction of it. Therefore, as the spectral variations as a function of the parameters are non-linear, the application of these $B_{\theta}^{\circ}(\lambda)$ functions will suffer from biases of variable importance, depending on the covered parameter range. On the other hand, a crucial characteristic of the stellar spectra grid is that non-linearity is almost negligible at a local scale of about 1000 K in T_{eff} , 1 dex in $\log g$ and 1 dex in $[M/H]$. Thus, if the errors introduced by the initial $B_{\theta}^{\circ}(\lambda)$ functions are equal to or smaller than the above mentioned limits, it is possible to converge to the correct

Table 1. Preliminary estimation of the parameters through initial MATISSE $B_{\theta}^{\circ}(\lambda)$ functions for the Gaia/RVS spectral domain and resolution. They correspond to spectra with $[M/H] > -3$ and $S/N > 25$. The $B_{\theta}^{\circ}(\lambda)$ functions are applied for a subgrid selection before the use of the final local $B_{\theta}^l(\lambda)$ functions.

	$T_{\text{eff}} < 4500\text{K}$	$4500 < T_{\text{eff}} < 6000\text{K}$	$T_{\text{eff}} > 6000\text{K}$
ΔT_{eff}	300-600 K	200-600 K	400-750 K
$\Delta \log g$	0.1-1.0 dex	0.1-0.3 dex	0.1-0.2 dex
$\Delta [M/H]$	0.1-0.5 dex	0.1-0.6 dex	0.2-0.6 dex

solution. This is, in fact, the case for the Gaia/RVS spectral domain and resolution (even if it contains rather few lines compared to other spectral regions more in the blue). Table 1 presents the corresponding errors coming from the application of the initial $B_{\theta}^{\circ}(\lambda)$ functions for flux calibrated spectra. Those values have been derived for the whole set of trial spectra and additionally verified for all the spectra of the grid with $[M/H] > -3.0$ dex. The first guess in the $[\alpha/\text{Fe}]$ is chosen as a function of the global metallicity value, following the same α -enhancements considered in Section 3.1.

The achieved precisions in the atmospheric parameters are clearly adequate for a subgrid selection and a subsequent refinement of the results using local $B_{\theta}^l(\lambda)$ functions. In addition, those values are practically the same at any signal to noise ratio, as the errors are largely dominated by the bias, which is due to non linearity problems and independent of the noise.

On the other hand, the number of initial $B_{\theta}^{\circ}(\lambda)$ functions can depend on the selected parameter and the values covered by the grid. In the case of the Gaia/RVS grid described in Section 3.1, only one $B_{T_{\text{eff}}}^{\circ}(\lambda)$ has been necessary to attain the objectives of accuracy for the selection of the local *almost linear* subgrids and the subsequent application of the final $B_{T_{\text{eff}}}^l(\lambda)$. On the contrary, the first guesses in gravity and metallicity are coupled to the preliminary estimation of temperature: four different $B_{\theta}^{\circ}(\lambda)$ functions and three $B_M^{\circ}(\lambda)$ functions were calculated, at different temperature intervals. The use of a rough temperature estimation in the preliminary evaluation of the other two atmospheric parameters tackles the problem of degeneracy between them and reduces the final set of initial $B_{\theta}^{\circ}(\lambda)$ functions to eight.

One possible alternative approach to the use of the initial $B_{\theta}^{\circ}(\lambda)$ functions could be the photometric estimation of a star's atmospheric parameters through available colours or the location on a colour-magnitude diagram.

The second step is the use of the local $B_{\theta}^l(\lambda)$ functions to derive the final stellar parameters. Once a centre of the subgrid has been chosen (e.g. $T_{\text{eff}} = 5750$ K, $\log g = 4.5$ dex, $[M/H] = 0.0$ dex, $[\alpha/\text{Fe}] = 0.0$ dex, for solar type stars) the computed $B_{\theta}(\lambda)$ functions, can be used to analyse object spectra whose atmospheric parameters and abundances are estimated to be near or inside the range covered by the subgrid. This includes any set of parameters, not necessary with an equivalent among the points of the grid (e.g. the Sun: $T_{\text{eff}} = 5777$ K, $\log g = 4.44$ dex, $[M/H] = 0.0$ dex, $[\alpha/\text{Fe}] = 0.0$ dex).

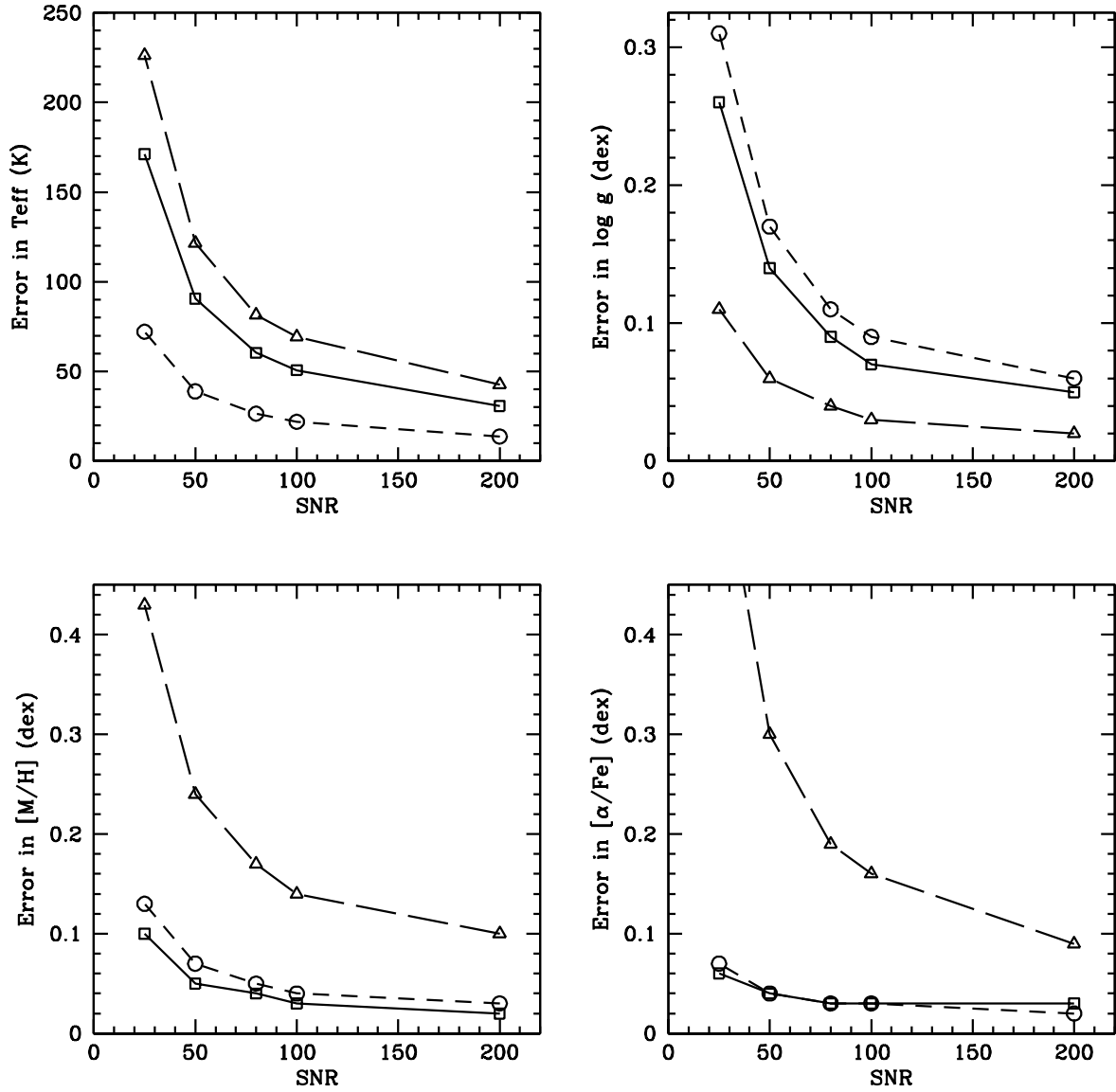


Figure 2. Mean maximum errors in the recovered parameters as a function of the S/N, for synthetic flux calibrated spectra in the Gaia/RVS domain. The three different lines on each panel correspond to metal rich cool dwarfs (solid line and squares), intermediate metallicity cool giants (short dashed line and circles), metal poor hot subgiants (long dashed line and triangles).

Figure 2 presents the mean maximum errors (mean bias plus mean standard deviation) in the recovered parameters (effective temperature, gravity, global metallicity and $[\alpha/\text{Fe}]$ content) as a function of the S/N, for the considered synthetic flux calibrated spectra in the Gaia/RVS domain. The three different lines on each panel correspond to above defined metal rich cool dwarfs (solid line and squares), intermediate metallicity cool giants (short dashed line and circles), metal poor hot subgiants (long dashed line and triangles). In the following, the results for the three types of stars are discussed.

3.3.1 Metal rich cool dwarfs

The results indicate very small mean error (bias) values at any S/N ratio: less than ~ 10 K for the effective temperature, less than ~ 0.03 dex for the gravity, less than ~ 0.03 dex for $[\text{M}/\text{H}]$ and $[\alpha/\text{Fe}]$. The total maximum error, as plotted on Fig. 2, includes, in addition, the mean standard deviation at each S/N value. For $\text{S/N} \geq 50$ it is smaller than ~ 90 K, 0.14 dex, 0.05 dex and 0.04 dex for T_{eff} , $\log g$, $[\text{M}/\text{H}]$ and $[\alpha/\text{Fe}]$ respectively. At lower signal to noise values, the reduced quantity of information makes the standard deviation increase, although the total errors remain at acceptable

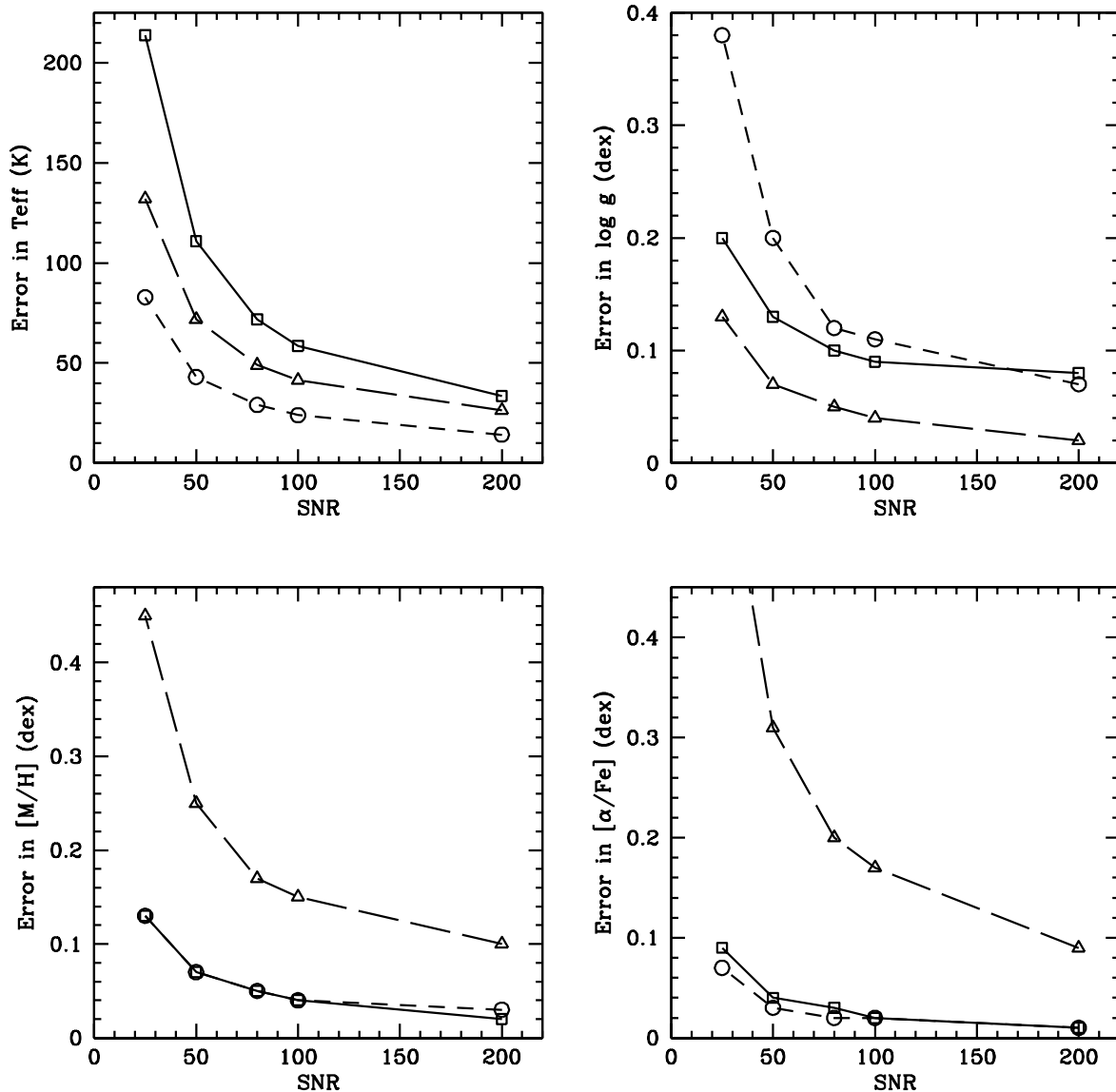


Figure 3. Mean maximum errors in the recovered parameters as a function of the S/N, for synthetic continuum normalized spectra in the Gaia/RVS domain. The symbols are the same of Fig. 2

levels down to S/N=25 (~ 173 K, 0.25 dex, 0.1 dex and 0.06 dex respectively).

3.3.2 Intermediate-metallicity cool giants

As in the previous case, no significant biases were found in the derived parameters. The more remarkable difference, with respect to solar type stars, is the higher accuracy on the T_{eff} determination. Basically, this is due to the fact that the $B_{T_{\text{eff}}}(\lambda)$ function has additional temperature indicators (mainly molecular lines) and that its amplitude variations are larger by more than a factor of two with respect to the solar case (more numerous spectral lines are more sensitive

to the effective temperature). On the other hand, although still very well determined, the errors in the other parameters reflect a slightly smaller sensitivity of the calcium lines and the Pa 14 line to $\log g$, and the smaller metal content of the analysed stars (with spectra having a smaller number and weaker available lines).

3.3.3 Very metal-poor hot subgiants

The analysis of this kind of stars is worsened by the huge decrease in the number and the intensity of metallic lines, leading to higher errors in the global metallicity and the $[\alpha/Fe]$ content. This is probably the most challenging case

for a chemical analysis, in general, due to the lack of information (nevertheless, $[M/H]$ and $[\alpha/Fe]$ content are still well determined when $S/N > 50$). In contrast, the Paschen lines are strengthened at this temperature and they allow a very accurate determination of the gravity and satisfactory results for the effective temperature.

3.4 Application to continuum normalized spectra

This section takes into account the more common situation of non flux calibrated spectra for which the continuum level is fitted by a polynomial to which the whole spectrum is then normalized. To this purpose, a new grid of continuum normalized synthetic spectra was computed. First of all, the MATISSE algorithm was applied to normalized synthetic spectra in order to study the effects, on the performances of the algorithm, of the loss of the information provided by the absolute stellar flux. Lastly, the observed continuum normalized spectra of two classical stars (the Sun and Arcturus) are analysed to exemplify the application to observed data.

3.4.1 Synthetic spectra

A data base of a hundred continuum normalized synthetic spectra, with the same randomly chosen parameters selected for the tests in Sect. 3.3, were treated. Again, 5 different S/N values and 1000 tests per signal to noise ratio were performed for each spectrum.

Figure 3 presents the corresponding mean maximum errors in the recovered parameters as a function of the S/N , with the same division as Fig. 2 on metal rich cool dwarfs, intermediate metallicity cool giants, metal poor hot subgiants.

First, we can note that the performances for the global metallicity and the $[\alpha/Fe]$ content are not influenced by the absence of flux calibration. This implies the possibility of deriving the $[M/H]$ and the α -element abundance with an accuracy better than 0.1 dex for most types of stars, even with rather poor quality spectra.

On the other hand, the loss of the information about the effective temperature contained in the stellar flux (also revealed by the slope of a $B_{T_{\text{eff}}}(\lambda)$ function for flux calibrated spectra, like that of Fig. 1) induces a small increment of the error (the standard deviation, not the bias) as the signal to noise decreases. Slight error increments are also observed for the gravity determination of cool dwarfs and giants. In any case, both temperature and gravity are still well determined for continuum normalized spectra.

3.4.2 Observed spectra

We present in the following two examples of the usage of MATISSE for the analysis of observed spectra, in order to justify and explain its application to real data treatment. As mentioned before, the analysis of observed spectra suffers from various effects that blur the extraction of the available information on a particular parameter: approximations in the computation of theoretical spectra, errors in the wavelength calibration, treatment of the line broadening, etc...

In order to check and illustrate the results of the algorithm under those possible complications, two stars with well

known atmospheric parameters and chemical abundances have been considered: the Sun and Arcturus (α Boo). In addition, they match two of the cases studied above through the tests with synthetic spectra: metal rich cool dwarfs and intermediate metallicity cool giants. The observed spectra have been taken from Hinkle et al. (2000) and their resolution was degraded to the Gaia/RVS one, with the same sampling as the synthetic spectra described in Section 3.1.

As already mentioned in Section 3.1, the validity of the considered line data and the classical assumptions used (LTE, hydrostatic) have not been checked here for all types of stars. Hence, biases on the derived parameters of observed stars are expected to be found. They can eventually be confirmed by a comparison between the results obtained for an observed spectrum, and those for a synthetic one with the same atmospheric parameters (without biases).

In the case of the Sun ($T_{\text{eff}} = 5777$ K, $\log g = 4.44$ dex, $[M/H] = 0.0$ dex, $[\alpha/Fe] = 0.0$ dex), the $B_{T_{\text{eff}}}^c(\lambda)$ functions provided a first parameter estimation with errors of 400 K, 0.34 dex and 1.2 dex in T_{eff} , $\log g$ and $[M/H]$ respectively. That allowed to converge, using the local $B_{T_{\text{eff}}}^l(\lambda)$ functions to the following solution: $T_{\text{eff}} = 5758$ K, $\log g = 4.33$ dex, $[M/H] = 0.07$ dex, $[\alpha/Fe] = -0.05$ dex.

For the Arcturus spectrum, the errors in the first parameter evaluation were 260 K, 0.20 dex and 0.9 dex in T_{eff} , $\log g$ and $[M/H]$ respectively. The final derived values for Arcturus were: $T_{\text{eff}} = 4277$ K, $\log g = 1.7$ dex, $[M/H] = -0.40$ dex, $[\alpha/Fe] = 0.15$ dex. These values can be compared to those published by Peterson et al. (1993): $T_{\text{eff}} = 4300 \text{ K} \pm 30 \text{ K}$, $\log g = 1.5 \pm 0.15$ dex, $[M/H] = -0.5 \pm 0.1$ dex, and $[\alpha/Fe]$ ranging from 0.3 ± 0.1 dex to 0.4 ± 0.1 dex, depending on the considered α -element.

Finally, as already mentioned, the small differences (bias) between the derived parameters for the Sun and Arcturus and those in the literature could arise from inadequations of the theoretical spectra, mainly implemented for the test of the algorithm. To verify this possibility, synthetic continuum-normalized spectra, with atmospheric parameters equal to those of the Sun and Arcturus, were calculated and treated with the same $B_{\theta}(\lambda)$ functions as the observed ones. The errors (biases) in the results were actually considerably smaller: for the synthetic Sun, $\Delta T_{\text{eff}} = 6$ K, $\Delta \log g = 0.02$ dex, $\Delta [M/H] = 0.01$ dex and $\Delta [\alpha/Fe] = 0.01$ dex; for the synthetic Arcturus, 1 K, 0.01 dex, 0.004 dex and 0.006 dex, respectively. As a consequence, we conclude that the small biases in the results presented here are most probably coming from imperfections in the physical assumptions and the line data used for the theoretical spectra computation. The suitability of the MATISSE algorithm to the analysis of observed spectra is therefore confirmed.

4 DISCUSSION AND CONCLUSIONS

The illustrated results corroborate the efficiency of the automated MATISSE algorithm as a spectral analysis and classification tool. In particular, the capabilities of MATISSE to accurately derive stellar atmospheric parameters and chemical abundances (as the $[\alpha/Fe]$ ratio) have been described. The method gives rapid, compelling and stable results, without biases, even for moderate to low signal to noise spectra and flux normalized data.

The accuracy values presented here correspond to a red spectral domain, that of the Gaia/RVS, where the number of metallic lines, and therefore the quantity of information, is smaller than at bluer wavelengths. Even better results could indeed be achieved in different spectral domains or by increasing the wavelength range of analysis or the spectral resolution. The stable performances for stars in different regions of the Hertzsprung-Russel diagram and the applications to chemical abundance determinations make of MATISSE a powerful tool for the study of stellar populations. In particular, the accuracies attained on chemical abundances are better than about 0.1 dex (except for very low-metallicity hot stars with too few available lines), as required to constrain Galactic formation and evolution models (see for example, Prantzos, 2003; Robin et al., 2000). Finally, no border effects (error increasing for object spectra with parameters near the limits of the considered spectra grid), with respect to the synthetic spectra grid, are disturbing the results, at variance with what is usually the case for minimum distances methods.

This algorithm represents a new effort in automated spectral analysis, different from the already existent automated classification techniques. In 1985, Cayrel de Strobel claimed, from theoretical considerations, that metallicity can be determined from high resolution spectra, of known effective temperature and gravity, with an accuracy of ± 0.07 dex at $S/N=250$ and of ± 0.2 dex at $S/N=50$. Later on, Jones et al. (1996) derived $[Fe/H]$ values for G stars, through the use of spectroscopic indices at 1\AA resolution in the range $4000\text{-}5000\text{\AA}$. They achieved errors of ± 0.2 dex at low S/N (10-20). Since then, the main efforts on automated stellar parameter determination could be divided in three categories: minimum distances techniques, genetic algorithms and neural networks. In this context, the method presented here opens an unexplored avenue.

The minimum distances technique was applied by Katz et al. (1998), using a template grid of flux calibrated observed spectra of FGK stars with solar composition, in a much larger wavelength range and at a higher spectral resolution than those presented here (a 2900\AA region around 5300\AA , with $R=42\,000$). They estimated the internal accuracy of their method to be 86 K, 0.28 dex and 0.16 dex for T_{eff} , $\log g$ and $[M/H]$ at $S/N=100$, that is, (except for T_{eff}) much higher errors than those achieved with MATISSE.

Bonifacio & Caffau (2003) performed an automated abundance analysis of giants in the Sagittarius dwarf-spheroidal galaxy using a χ^2 technique. They achieved an accuracy in the $[Fe/H]$ determination of 0.18 dex, for spectra of stars with known T_{eff} and $\log g$, $R=15\,000$ and $S/N=20$. Some stability problems at low metallicity are also reported.

Allende Prieto (2003) applied a genetic algorithm to determine stellar atmospheric parameters from spectra, in a 150\AA region around $H\beta$, of A- to K-type stars with $S/N \simeq 150$. The estimated 1σ errors for $R \simeq 5000$ resolution, are 100 K, 0.3 dex, 0.1 dex for T_{eff} , $\log g$ and $[Fe/H]$, respectively.

A growing number of works have been developed using artificial neural networks. Bailer-Jones (2000) reports, for very low resolution ($R=60\text{-}100$) and low signal to noise ($S/N=5\text{-}10$) spectra, in a very large wavelength domain (a 7000\AA region, centered on 6500\AA) errors of 50-300 K in T_{eff} , ≥ 0.2 dex in $\log g$ and 0.2 dex in $[M/H]$, across practically the whole HR diagram. Snider et al. (2001) tested the appli-

cation of artificial neural networks on a sample of G- and F-type stars, with spectra in a $\sim 850\text{\AA}$ domain in the blue, at medium resolution ($R=2000\text{-}4000$). They attained accuracies of 135-150 K, 0.25-0.30 dex and 0.15-0.20 dex in effective temperature, gravity and $[Fe/H]$, respectively. Lastly, Willensen et al. (2005) employed feed forward neural networks, trained on synthetic spectra in a 1800\AA region around 4700\AA ($R \simeq 1500\text{-}2400$), to determine metallicities of main-sequence turn-off, subgiant and red giant stars in two globular clusters. They reported uncertainties, for $S/N=40\text{-}80$, of 140-190 K in T_{eff} , 0.3-0.4 dex in $\log g$ and 0.15-0.2 dex in $[Fe/H]$.

At variance with genetic algorithms and artificial neural networks, the automated method presented here exploits the possibility of easily selecting a parameter domain (the grid subregion) where the spectrum variations are practically linear. Summing up, the performances of the MATISSE algorithm are better or, at least, comparable to previous results on automated analysis, for different spectral domains and resolutions. They are also competitive with the results obtained by fine analysis of high-resolution spectra. In addition, $[\alpha/Fe]$ automated derivations are presented for the first time, with very positive results. The MATISSE algorithm could be applied also to a classification based on photometric indices or spectra of non resolved galaxies.

On another hand, regarding the computational time needed to derive the atmospheric parameters of an unknown star, the efficiency of the MATISSE algorithm is very high. Indeed, once the $B_\theta(\lambda)$ have been derived for different locations of the HR diagram (or subgrids), the stellar parameters are almost instantaneously derived from Eq. 1. For each parameter, only a multiplication of two vectors which dimension is equal to the number of sampling elements in the spectra has to be carried out. As a consequence, the atmospheric parameters and the $[\alpha/Fe]$ content of the whole Gaia/RVS spectra database could be evaluated in about 1 hour, with only one present day processor running at 0.5GFLOP/sec. On the other hand, the derivation of the $B_\theta(\lambda)$ functions (covariance matrix calculation between the spectra of the grid and solution of Eq. 6) takes less than 1 month of computational time with one present day technology 0.5GPLOP/s processor, for the case of the grid presented in Section 3.1. This time can be exactly divided by the number of available processors, as the different $B_\theta(\lambda)$ functions are calculated independently (e.g. ~ 1 week of computing time with 4 processors).

We can finally conclude that MATISSE is particularly adapted to the analysis of large surveys with huge amount of spectra, as the Gaia mission. Further applications of the algorithm, as the measurement of individual stellar chemical abundances, stellar rotation and microturbulence, will be implemented in the future. This will allow to generalize and exploit, as much as possible, the capabilities of the MATISSE algorithm on stellar spectra analysis.

ACKNOWLEDGMENTS

We thank the MARCS collaboration for providing us the grid of model atmospheres in advance of publication and B. Plez for his molecular line lists and tools for computing stellar spectra. The VALD database was used for the atomic

lines. J.C. Gazzano is acknowledged for his help with Fig. 1 of this paper and we are grateful to D. Katz for discussions and advices regarding the Gaia Radial Velocity Spectrograph. We acknowledge F. Thévenin for his initial interest in this work. We sincerely thank the anonymous referee whose corrections and advices have sensitively improved this paper. ARB acknowledges the support of the European Space Agency.

REFERENCES

- Allende Prieto, C., 2003, MNRAS, 339, 1111
 Alvarez, R., & Plez, B. 1998, A&A, 330, 1109
 Asplund, M., 2005, ARA&A, 43, 481
 Asplund, M., Grevesse, N., Sauval, A.J., 2005, ASPC, 336, 25
 Bailer-Jones C.A.L., Irwin M., von Hippel T., 1998, MNRAS 298, 361
 Bailer-Jones, C.A.L., 2000, A&A 357, 197
 Bailer-Jones, C.A.L., 2001, in Gupta R., Singh H. P., Bailer-Jones C.A.L., eds, Proc. Automated data analysis in Astronomy. Narosa Publishing House, New Delhi, India, p. 83
 Barklem P.S., Piskunov N., O'Mara B.J., 2000, A&AS 142, 467
 Bonifacio, P. & Caffau, E., 2003, A&A, 399, 1183
 Cayrel, R., Depagne, E., Spite, M., et al. 2004, A&A, 416, 1117
 Cayrel de Strobel G., 1985, In: Hayes D.S., Pasinetti L.E., Davis Philip A.G. (eds.) IAU Symp. 111, Calibration of Fundamental Stellar Quantities. Reidel, Dordrecht, p. 137.
 Grevesse, N., & Sauval, A.J. 1998, Space Science Reviews, 85, 161
 Gustafsson, B., et al., 2003, in "Modelling of stellar atmospheres", IAU symposium 210, Piskunov, Weiss and Gray eds., ASP pub., A4
 Gustafsson, B., et al., 2006 in preparation
 Hinkle et al., 2000, IAUJD 1E, 26
 Jones J.B., Gilmore G., Wyse R.F.G., 1996, MNRAS 278, 146
 Katz, D. et al. 1998, A&A 338, 151
 Kupka, F., Piskunov, N.E., Ryabchikova, T.A., Stempels, H.C., Weiss, W.W. 1999, A&AS 138, 119
 Munari, 2003, ASP. Conference Proceedings, 298, 51. Edited by Ulisse Munari.
 Peterson, R. C., Dalle Ore, C. M., Kurucz, R. L., 1993, ApJ, 404, 333
 Prantzos, 2003, A&A, 404, 211
 Querci, F., Querci, M., Kunde, V.G. 1971, A&A, 15, 256
 Recio-Blanco, A. et al., 2005, Proceedings of the Gaia Symposium *The Three-Dimensional Universe with Gaia* (ESA SP-576), p. 615. Editors: C. Turon, K.S. O'Flaherty, M.A.C. Perryman.
 Recio-Blanco, A., de Laverny, P., Plez., B., 2005, European Space Agency technique note RVS-ARB-001
 Robin et al., 2000, A&A, 359, 103
 Snider et al., 2001, ApJ 562, 528
 Thévenin, F., Bijaoui, A. & Katz, D., 2003, ASP. Conference Proceedings, 298, 291. Edited by Ulisse Munari.
 Van Cittert, P.H., 1931, Zeitschrift für Physik, 69, 298
 Weaver Wm.B. & Torres-Dodgen A.V., 1995, ApJ 446, 300
 Weaver Wm.B. & Torres-Dodgen A.V., 1997, ApJ 487, 847
 Willemsen, P.G. et al., 2003, A&A, 401, 1203
 Willemsen, P.G. et al., 2005, A&A 436, 379

This paper has been typeset from a $\text{T}_{\text{E}}\text{X}/\text{L}^{\text{A}}\text{T}_{\text{E}}\text{X}$ file prepared by the author.